Finding Structure in the Speed of Sound of Supranuclear Matter from Binary Love Relations

Hung Tan,[1] Veronica Dexheimer,[2] Jacquelyn Noronha-Hostler,[1] and Nicolás Yunes[1]
[1]Illinois Center for Advanced Studies of the Universe, Department of Physics, University of Illinois at Urbana-Champaign, Urbana, Illinois 61801, USA
[2]Department of Physics, Kent State University, Kent, Ohio 44243, USA

(Received 18 November 2021; accepted 16 March 2022; published 18 April 2022)

Analyses that connect observations of neutron stars with nuclear-matter properties can rely on equation-of-state insensitive relations. We show that the slope of the binary Love relations (between the tidal deformabilities of binary neutron stars) encodes the baryon density at which the speed of sound rapidly changes. Twin stars lead to relations that present a signature "hill," "drop," and "swoosh" due to the second (mass-radius) stable branch, requiring a new description of the binary Love relations. Together, these features can reveal new properties and phases of nuclear matter.

DOI: 10.1103/PhysRevLett.128.161101

Introduction.—Neutron stars (NSs) contain the highest possible densities known to humanity within their core. The maximum baryon density can reach up to 10 times nuclear saturation ($\rho_{\rm sat} \equiv m_N n_{\rm sat} \approx 2.7 \times 10^{14}$ g cm^{-3}, with m_N the nucleon mass and $n_{\rm sat} \equiv 0.16$ fm^{-3} the baryon number density at saturation). As a consequence, their cores may contain baryon resonances, hyperons, and deconfined quarks. It is not yet clear if the appearance of these new degrees of freedom would be related to smooth crossovers or *nth*-order phase transitions. Here we explore specific features in the equation of state (EOS) to phase transitions that lead to observable features in the binary Love relations (BLR) of NSs [1–3]. In this way, we can use astrophysics to learn about new features and phases of dense matter.

For first-order phase transitions, additional stable branches may appear in mass-radius sequences giving rise to *mass twins* [4–34], ie., NSs with nearly the same mass but different radii. For crossovers, large "bumps" in the speed of sound ($c_s^2 \equiv dp/d\epsilon$, where p is pressure and ϵ energy density) can appear [8,17,19–25,35–61]. A fast increase in c_s^2 points to a rapid change in the characteristics of strongly interacting matter, due to the (i) appearance of strangeness or more massive degrees of freedom, (ii) change in effective degrees of freedom, (iii) restoration or breaking of symmetries, and (iv) strengthening or weakening of different strong interactions. Reason (i) could be related to stiff EOSs suddenly softening due to the appearance of hyperons, resonances, or strange quarks (e.g., Fig. 2 in Ref. [9] and Refs. [8,17,19,35,36,40,41,46–53,62–74]. Reason (ii) could be related to first-order phase transitions [39,45,53,75–79] or an "unphase transition," as predicted by the quarkionic model [36,41,43,49,80,81] or crossover transitions and Gibbs constructions with (stiff) quark matter [37,38,46,52,82–85]. Reason (iii) could be associated with chiral symmetry (predicted by QCD to be restored at large densities) [55,82,86,87] or symmetries related to different pairing schemes [19,47]. Reason (iv) could be related to the behavior of different meson condensates [48].

Gravitational wave (GW) observations may reveal the complexity of matter at high densities through inferences on the masses and tidal deformabilities of NSs in coalescing binaries. In a binary, the gravitational field of one star perturbs the field of the other and vice versa, speeding up their inspiral. Since GWs are generated by accelerations, this change in the inspiral rate is encoded in the GWs emitted, which carry information about the NS tidal deformabilities $\Lambda_{1,2}$. Thus, a sufficiently loud signal allows for a measurement of a certain combination of $\Lambda_{1,2}$, the chirp tidal deformability $\tilde{\Lambda}$. One method to extract $\Lambda_{1,2}$ from $\tilde{\Lambda}$ is through EOS-insensitive BLR [1–3,88,89]. Once Λ_1 and Λ_2 have been inferred, one can then use a second EOS-insensitive "Love-C" relation between $\Lambda_{1,2}$ and the compactness $\mathcal{C}_{1,2} \equiv M_{1,2}/R_{1,2}$ (stellar mass over radius) to infer the individual compactnesses. From these, and separate inferences about the component masses encoded in other parts of the GW, one can infer the individual radii of the NSs [3,88,89]. These EOS-insensitive relations were originally derived using a vast array of EOSs that do not present features such as bumps in c_s^2, nor do they allow for mass twins. Could it be that the structure in the c_s^2 imprints onto the EOS-insensitive relations, which could be observed with inspiraling NSs? This is the question we tackle here.

Methodology.—We follow the formalism in Ref. [9] to model the EOS, which consists of three parts: a "crust" (loosely defined as the low density EOS $n \lesssim 1.5 n_{\rm sat}$), structure functions, and transition functions. For the crust,

we use the SLy EOS [90–92]. Beyond that, a bump and/or plateau is introduced in c_s to mimic different-order phase transitions. Transition functions are used to connect different parts of the EOS smoothly [9,93].

We then follow Refs. [1,2] to calculate the mass, radius, and tidal deformabilities of nonrotating NSs in a binary system during the late quasicircular inspiral. At zeroth-order in perturbation theory, the Einstein equations reduce to the Tolman-Oppenheimer-Volkov equations, which we solve numerically to find the radius and the mass for a given central density. At first order in perturbation theory, we solve the linearized Einstein equations to find the (electric-type, quadrupole) tidal deformability, defined as minus the ratio of the induced quadrupole moment to the external quadrupole tidal field. We then nondimensionalize this quantity to compute the dimensionless tidal deformability Λ at a given central density. Considering a sequence of central densities for a given EOS, we can then construct a mass-radius curve, a Love-C curve, and for a fixed mass ratio, the BLRs $\Lambda_a(\Lambda_s)$, defined with the symmetric and antisymmetric tidal deformabilities $\Lambda_{s,a} = (\Lambda_1 \pm \Lambda_2)/2$ [1,2].

Mass and radius without first-order phase transitions.—Consider NSs with EOSs that present structure in c_s^2 with higher (than first)-order phase transitions. Panel (a) of Fig. 1 shows c_s^2 for four EOS models. The first three present a steep rise in c_s^2 that starts around $n \lesssim 1.5 n_{\rm sat}$, followed either by a plateau at the causal limit or a bump that returns to the conformal limit. EOS 4 presents a bump similar to that of EOS 1, but at a larger number density ($n \sim 3 n_{\rm sat}$).

The corresponding mass-radius curves are shown in panel (b) of Fig. 1. EOSs that have a steep rise in c_s^2 at densities of $n \gtrsim 3 n_{\rm sat}$ lead to heavy NSs where the mass-radius curves bend toward the left (i.e., $dM/dR < 0$ for EOS 4). In contrast, EOSs with a steep rise in c_s^2 at lower densities produce mass-radius sequences that bend to the right (i.e., $dM/dR > 0$ for EOSs 1–3). Why is this? A sharp rise in c_s^2 implies a faster increase of pressure with baryon density. If the sudden rise happens at low density, i.e., somewhere relatively close to the stellar surface, the pressure inside the NS is larger than it would be otherwise, which increases the NS radius. Such an increase in R changes the slope dM/dR from very large in absolute value and negative (EOS 4) to not as large and positive (EOSs 1–3).

Rises at densities below $n < 1.5 n_{\rm sat}$ may also produce $dM/dR > 0$ sequences. These, however, are much more constrained because such rises produce EOSs with a large symmetry energy slope L and fluffy stars, often outside constraints of the LVC collaboration and NICER. Thus, any rise in c_s^2 at low densities must be significantly smaller and accompanied by a previously mentioned EOS softening to fit within known constraints, leading to a smaller $dM/dR > 0$ [94]. One method of circumventing this is to place a significant first-order phase transition around $n_{\rm sat}$, followed by a steep rise.

The slope.—Using the same EOSs without first-order phase transitions, we can compute the dimensionless tidal deformabilities of two stars in a binary, and for a fixed mass ratio we can plot the BLR, shown in panel (c) of Fig. 1. These are linear relations, as expected from Refs. [1,2], but the slope is different when using EOSs with bump structure at low densities. The results are shown for a fixed mass ratio, $q \equiv M_1/M_2 = 0.75$, but we have verified numerically that the qualitative behavior is generic. The slope is independent of the bump height (EOS 1 vs 2), or whether the structure itself is a bump or a plateau (EOS 1 vs 3). The slope, however, does encode the number density at which the structure first appears (as shown by the change in slope between EOSs 1, 2, 3 vs 4).

Why does the slope of the BLRs depend on where the structure in c_s^2 is first introduced? One can construct an analytic expression for the tidal deformability of the form $\Lambda = \Lambda(\mathcal{C}, y)$ (e.g., Refs. [1,2]), which depends both on the

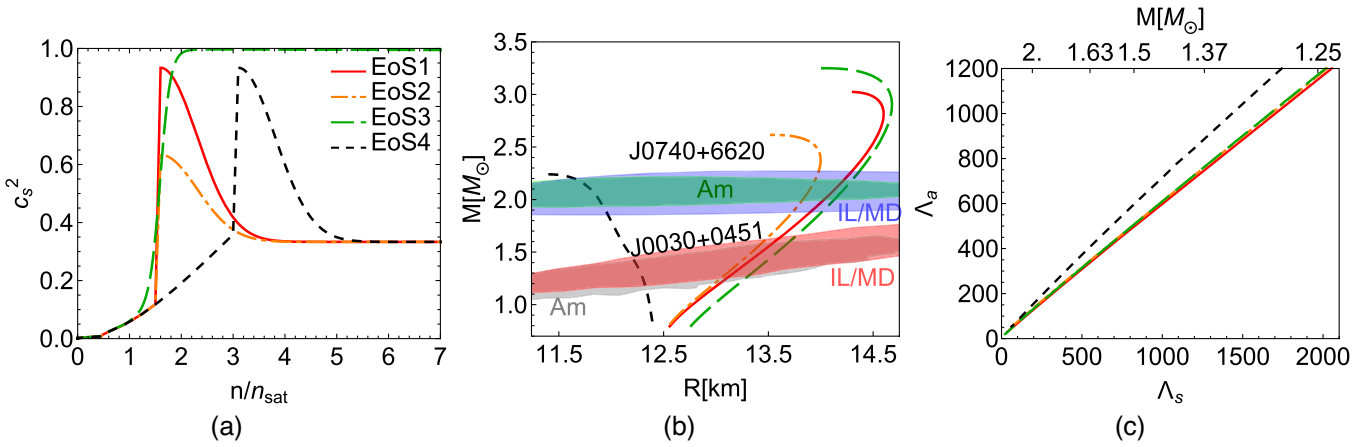

FIG. 1. c_s^2 as a function of $n/n_{\rm sat}$ (a), mass-radius curves (b), and BLRs for a mass ratio of $q = 0.75$ (c) for 4 EOS models. Structure in the EOSs near saturation bends the mass-radius curves to larger radii, while still being consistent with the two NICER observations at 90% confidence (Amsterdam or Illinois-Maryland).

compactness and a dimensionless quantity $y \equiv Rh_2'(R)/h_2(R)$, where h_2 is related to the (t,t) component of the metric. This quantity must be computed after solving the linearized Einstein equations for h_2, whose value at the stellar surface depends on integration constants that must be chosen to ensure the interior and exterior solutions are continuous at the surface. While y depends on both the central density and EOS, one can fit it to a polynomial in compactness $y = 1 + \sum_{n=1} a_n \mathcal{C}^n$, with EOS-dependent coefficients a_n.

Evaluating this expression for star 1 and star 2 in a binary, we can then compute the ratio Λ_a/Λ_s. The resulting expression is unilluminating, but to understand the change in slope of the BLR, it suffices to consider an expansion in $\mathcal{C}_{1,2} \ll 1$:

$$\frac{\Lambda_a}{\Lambda_s} = \frac{\mathcal{C}_2^5 - \mathcal{C}_1^5}{\mathcal{C}_2^5 + \mathcal{C}_1^5} + \frac{5(3+a_1)}{2}\frac{\mathcal{C}_1^5\mathcal{C}_2^5(\mathcal{C}_2 - \mathcal{C}_1)}{(\mathcal{C}_1^5 + \mathcal{C}_2^5)^2} + \mathcal{O}(\mathcal{C}_{1,2}^3), \quad (1)$$

which is consistent with the fact that $\Lambda_{1,2} \sim \mathcal{C}_{1,2}^{-5}$ when $\mathcal{C}_{1,2} \ll 1$, as shown in Refs. [1–3]. We see that, to leading order in $\mathcal{C}$, Λ_a/Λ_s is a constant related to the difference in compactness of the stars in the binary. A linear regression of the data used in panel (c) of Fig. 1 reveals that $(\Lambda_a/\Lambda_s)_{\rm lin.reg} \approx 0.57$ for EOSs 1–3 and $(\Lambda_a/\Lambda_s)_{\rm lin.reg} \approx 0.65$ for EOS 4, while our approximation above gives $(\Lambda_a/\Lambda_s)_{\rm Newt} \approx 0.56$ for EOSs 1–3 and $(\Lambda_a/\Lambda_s)_{\rm Newt} \approx 0.64$ for EOS 4. Equation (1) matches the fully numerical BLRs to better than $\lesssim 15\%$ for $\Lambda_s > 300$.

We have shown that the BLRs are given approximately by the difference in compactness, but we have yet to show how this relates to the slope of the mass-radius curve. For masses sufficiently smaller than the maximum mass, we can approximate the radius as a Taylor expansion $R_2 = R_1 + (dR/dM)_1(M_2 - M_1) + \mathcal{O}[(M_2 - M_1)^2]$, where here $M_2 > M_1$, but R_2 can be either larger or smaller than R_1 depending on the sign of the inverse slope $(dR/dM)_1$. Since dM/dR is large for NSs, then dR/dM is small (and not of $\mathcal{O}(1/\mathcal{C})$), and so we can write

$$\mathcal{C}_2 = \frac{\mathcal{C}_1}{q}\left[1 - \mathcal{C}_1\left(\frac{dR}{dM}\right)_1\left(\frac{1}{q} - 1\right) + \mathcal{O}(\mathcal{C}_1^2)\right]. \quad (2)$$

The leading-order term in the slope of the BLRs is then

$$\frac{\Lambda_a}{\Lambda_s} \approx \frac{\mathcal{C}_2^5 - \mathcal{C}_1^5}{\mathcal{C}_2^5 + \mathcal{C}_1^5} = \frac{1-q^5}{1+q^5} - 10\mathcal{C}_1\left(\frac{dR}{dM}\right)_1\frac{q^4(q-1)}{(q^5+1)^2} + \mathcal{O}(\mathcal{C}_1^2). \quad (3)$$

The slope of the BLRs clearly depends on the slope of the mass-radius curve. When dM/dR is negative (i.e., EOS 4), then the second term in Eq. (3) is positive, and therefore increases the slope. When dM/dR is positive (EoSs 1–3), then the second term in Eq. (3) negative, and therefore decreases the slope, as shown in panel (c) of Fig. 1.

What physical mechanisms produce such changes in a realistic EOS? Several scenarios have already been discussed in the introduction. In particular, we have tested the inclusion of a higher-order vector ω^4 interaction in the Chiral Mean Field model [69], which changes c_s^2 by introducing a rise at $n_B \sim 2n_{\rm sat}$ and, in turn, changes the slope of the mass-radius curve at small to intermediate masses (below 1.5 $M_\odot$). The inclusion of another vector interaction with isovector components ω–ρ softens the EOS around $n_B \sim n_{\rm sat}$, forcing c_s^2 to become small, followed by a steep rise. This decreases the radii of low-mass stars, tilting the mass-radius curve to the right and decreasing the slope of the BLRs (verified using the NL3 model [94,95]). A similar situation arises for pure (self-bound) quark stars [96], which also exhibit a dramatic $dM/dR < 0$ behavior [97]. While there are subtleties in the understanding of the physical mechanism that produces $dM/dR < 0$, in all cases it leads to a larger slope in $\Lambda_a(\Lambda_s)$.

Mass and radius with first-order phase transitions.—Figure 2(a) shows c_s^2 for various EOSs that reproduce mass-radius curves with a second stable branch [Fig. 2(b)]. The first-order phase transition occurs when $c_s^2 = 0$. All EOSs are allowed by NICER's observations of J0030 + 0451 and J0740 + 6620 to 90% confidence [98–101]. The introduction of structure at low number density changes the slope of

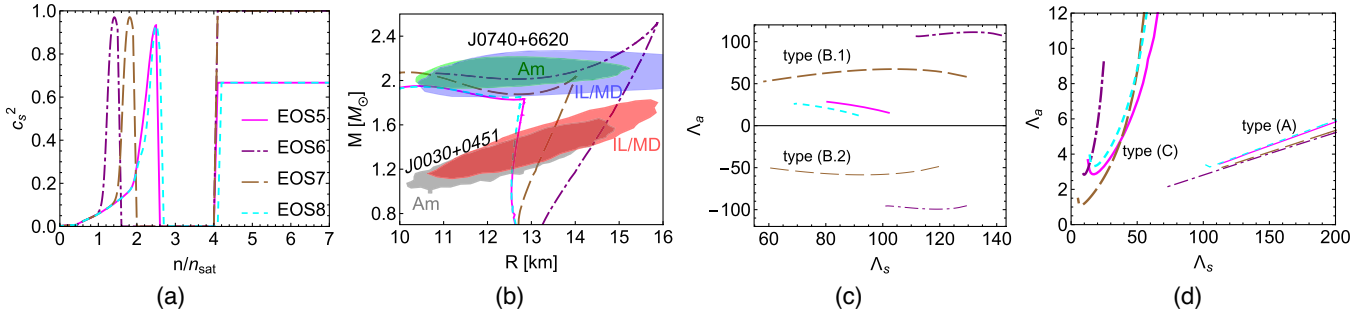

FIG. 2. Same as Fig. 1 but for EOSs that contain first-order phase transitions and a binary system with mass ratio $q = 0.99$. The first-order phase transitions ($c_s = 0$) of panel (a) introduce a second stable branch in the mass-radius curves (b). BLRs between stars in the same or different branches produce a slope, hill, drop, and swoosh (c),(d).

the mass-radius curve, and allows for massive stars. This impacts both the first and second stable branches.

There are three relevant cases in the BLRs of mass twins: type A, with both stars in the first branch; type B, with one star in the first and one in the second branch; and type C, with both stars in the second branch. Type A binaries present BLRs similar to the above discussion, while type B and C binaries lead to different behavior [102].

The hill and the drop.—Figure 2(c) shows the BLR for type B.1 binaries with thick curves [i.e., the less massive star (M_1) in the first branch and the more massive one (M_2) in the second] and for type B.2 binaries with thin curves (vice versa).

For type B.2 binaries, $\Lambda_a \propto \Lambda_1 - \Lambda_2 < 0$, but for type A, $\Lambda_a > 0$. This is because for type A binaries the most massive star is harder to deform, so it has a lower Λ, i.e., $\Lambda \propto C^{-p}$ with $p > 0$. In type B.2 binaries, the lighter star is significantly more compact because it is in the second branch; thus, the lighter star is harder to deform.

Not all EOSs lead to type B.2 binaries. For the latter to exist, we must have the more massive star in the first branch, and the less massive star in the second branch. This is not possible for EOSs where most stars in the second branch are heavier than those in the first branch (e.g., the turquoise dashed curve and the pink solid curve in Fig. 2).

The BLRs of type B.1 binaries can present either a "drop" (i.e., a nearly straight line with negative slope), or a "hill" (i.e., a nearly concave-down quadratic with a wide summit). The Love number always increases when mass decreases, but the Love-M relations in the first and second branch have different derivatives with respect to mass. For stars in the first branch, $|d\Lambda/dM|$ is nearly constant, but for stars in the second branch, this is not the case. For low-mass stars with certain EOSs (e.g., EOSs 6 and 7), the magnitude of the derivative is larger in the second branch than in the first branch, but then it becomes smaller at larger masses; this is what causes the hill-like feature in the BLR. For other EOSs (EOSs 5 and 8), $|d\Lambda/dM|$ is always larger for stars in the second branch than in the first branch, leading to the drop in the BLRs.

The inverted hill BLR of type B.2 binaries is nearly a mirror image of the hill BLR of type B.1 binaries. This is not an exact symmetry but it is good to $\lesssim 30\%$. This is because for both type B.1 and B.2 binaries, the Love-M relation for the star in the second branch is the same concave quadratic. Although the Love-M relation for the star in the first branch is nearly a straight line in both types of binaries, they could be shifted to lower Λ_s. The shift, however, is very small because the compactness range in the first branch of B.1 and B.2 binaries is similar, due to the small mass ratio required for type B binaries to exist.

The swoosh.—Since both stars in type C binaries are in the second stable branch, only a small range of masses is possible, forcing $q \sim 1$. Type C stars should break universality because the BLRs are only EOS insensitive when the mass ratio is away from unity [1,2]. Figure 2(d) confirms this expectation and shows a "swoosh," i.e., a nonlinear curvature in the BLRs that can be mathematically represented as a quadratic with an asymmetric domain.

When both stars are in the second branch, the swoosh appears at $\Lambda_a \in (1, 8)$, while when both stars are in the first branch, the swoosh is smaller, and it appears only for specific EOSs, as shown in Fig. 2(d) This is because for the swoosh to appear, $\Lambda_{1,2}$ has to be quite small, and so the NS masses must be large, which only happens for select EOSs. The swoosh also technically appears for binaries with EOSs without first-order phase transitions, provided the maximum mass is high enough, but it is an order of magnitude smaller.

All stars in the second branch are near the maximum mass. Therefore, an expansion in small compactness is not applicable. Instead, we must consider how $\Lambda_{1,2}$ scales with $\mathcal{C}_{1,2}$ in this high-mass regime. We find numerically that $\Lambda_{1,2} \propto \mathcal{C}_{1,2}^{-9}$ for stars in the second branch (instead of $\Lambda_{1,2} \propto \mathcal{C}_{1,2}^{-5}$, which is only valid when $\mathcal{C} \ll 1$). Equation (1) must be modified to $\Lambda_a/\Lambda_s = (\Lambda_1 - \Lambda_2)/(\Lambda_1 + \Lambda_2) = (\mathcal{C}_1^{-9} - \mathcal{C}_2^{-9})/(\mathcal{C}_1^{-9} + \mathcal{C}_2^{-9})$, not requiring $\mathcal{C} \ll 1$.

Further progress necessitates a relation between the compactnesses of two stars in the second branch. Since $q \sim 1$, we can use Eq. (2) to write $\mathcal{C}_1 = b\Lambda_2^{-1/9} q[1 + b\Lambda_2^{-1/9} \times (\Delta R/\Delta M)_1 \delta + \mathcal{O}(\delta^2)]$, where $\delta = 1 - q \ll 1$, $\mathcal{C}_{1,2} = b\Lambda_{1,2}^{-1/9}$, ΔM (ΔR) the mass (radius) difference between the two stars in the binary, and $b \approx 0.35$. Taylor expanding,

$$\Lambda_a = \frac{9}{2}\delta\left[\Lambda_s - b\frac{\Lambda_s^{8/9}}{(\Delta M/\Delta R)}\right] + \mathcal{O}(\delta^2). \tag{4}$$

This approximate BLR is controlled by the two terms inside the square bracket, with the size of $\Delta M/\Delta R$ dictating which term dominates. In the second branch, the slope $\Delta M/\Delta R$ is initially very small for the lowest mass stars (corresponding to large Λ_s). As one increases the central density (increasing mass, decreasing Λ_s), the slope $\Delta M/\Delta R$ reaches a maximum of $\mathcal{O}(10^{-1})$. An increase in central density beyond this decreases Λ_s and $\Delta M/\Delta R$ further, as the maximum mass is approached. Therefore, for large values of Λ_s [of $\mathcal{O}(10^2)$] and for small values of Λ_s [of $\mathcal{O}(1)$], the second term dominates because $\Delta M/\Delta R$ is small. For intermediate values of Λ_s [of $\mathcal{O}(10)$], both terms contribute roughly equally. This behavior causes the swoosh, and since it depends on $\Delta M/\Delta R$, its location is not EOS independent, as shown in Fig. 2(d).

Implications.—We have presented new physical properties of several features in the BLRs (a change in slope, a hill, a drop, and a swoosh) that encode nuclear physics information. Can these features be extracted from GW observations? The accuracy to which the tidal deformabilities can be extracted has been studied extensively [103]. During the fifth LIGO observing run ($O5$), one expects to

measure $\Lambda_{1,2}$ with uncertainties of $\delta\Lambda_{1,2} \approx 50$–$100$, while 3G detectors may allow measurements with uncertainties $\delta\Lambda_{1,2} \approx 5$–$10$ for an event similar to GW170817. The change in slope in the BLRs may be observable already during $O5$ if a sufficiently loud (SNRs around 100) and low-mass NS binary is detected, maybe allowing for a measurement of a rise in c_s^2 below $3n_{\rm sat}$.

The detection of the hill, drop, or swoosh would be a smoking gun signal of mass twins, but the detectability of the latter two is more challenging. The drop and the swoosh occur at very small Λ_a. Such a detection would require uncertainties in the measurements of $\Lambda_{1,2}$ of $\delta\Lambda_{1,2} \approx 1$ and ≈ 10, respectively. This is beyond both 2G and 3G detectors, unless an exceptionally loud signal is observed (e.g., a galactic source with SNRs in the 1000s). The hill structure may be detectable during $O5$ for a GW170817-comparable signal, if the NSs are sufficiently massive. The standard approximate universal BLRs [1,3,104] would not capture the hill, so their implementation in parameter estimation [88] would have to be revised. The detection of the hill would decisively determine that there is a first-order phase transition inside NSs, pointing toward the existence of deconfined quarks in the universe.

This work was supported in part by the NSF within the framework of the MUSES collaboration, under Grant No. OAC-2103680. J. N. H. acknowledges the support from the US-DOE Nuclear Science Grant No. DE-SC0020633. H. T. and N. Y. acknowledge support from NASA Grants No. NNX16AB98G, No. 80NSSC17M0041, and No. 80NSSC18K1352 and NSF Grant No. 1759615. V. D. acknowledges support from the National Science Foundation under Grants No. PHY-1748621 and No. NP3M PHY-2116686, and PHAROS (COST Action CA16214). The authors also acknowledge support from the Illinois Campus Cluster, a computing resource that is operated by the Illinois Campus Cluster Program (ICCP) in conjunction with the National Center for Supercomputing Applications (NCSA), and which is supported by funds from the University of Illinois at Urbana-Champaign.

[1] K. Yagi and N. Yunes, Phys. Rev. D **88**, 023009 (2013).
[2] K. Yagi and N. Yunes, Science **341**, 365 (2013).
[3] K. Yagi and N. Yunes, Classical Quantum Gravity **33**, 13LT01 (2016).
[4] S. Benic, D. Blaschke, D. E. Alvarez-Castillo, T. Fischer, and S. Typel, Astron. Astrophys. **577**, A40 (2015).
[5] J.-E. Christian and J. Schaffner-Bielich, Phys. Rev. D **103**, 063042 (2021).
[6] S. Han and M. Prakash, Astrophys. J. **899**, 164 (2020).
[7] P. T. H. Pang, T. Dietrich, I. Tews, and C. Van Den Broeck, Phys. Rev. Research **2**, 033514 (2020).
[8] P. Jakobus, A. Motornenko, R. O. Gomes, J. Steinheimer, and H. Stoecker, Eur. Phys. J. C **81**, 41 (2021).
[9] H. Tan, T. Dore, V. Dexheimer, J. Noronha-Hostler, and N. Yunes, Phys. Rev. D **105**, 023018 (2022).
[10] M. G. Alford, S. Han, and M. Prakash, Phys. Rev. D **88**, 083013 (2013).
[11] M. G. Alford, G. F. Burgio, S. Han, G. Taranto, and D. Zappalà, Phys. Rev. D **92**, 083002 (2015).
[12] M. G. Alford and S. Han, Eur. Phys. J. A **52**, 62 (2016).
[13] I. F. Ranea-Sandoval, S. Han, M. G. Orsaria, G. A. Contrera, F. Weber, and M. G. Alford, Phys. Rev. C **93**, 045812 (2016).
[14] S. Han and A. W. Steiner, Phys. Rev. D **99**, 083014 (2019).
[15] K. Chatziioannou and S. Han, Phys. Rev. D **101**, 044019 (2020).
[16] D. Blaschke and M. Cierniak, Astron. Nachr. **342**, 227 (2021).
[17] V. Dexheimer, R. Negreiros, and S. Schramm, Phys. Rev. C **91**, 055808 (2015).
[18] I. N. Mishustin, M. Hanauske, A. Bhattacharyya, L. M. Satarov, H. Stoecker, and W. Greiner, Phys. Lett. B **552**, 1 (2003).
[19] M. G. Alford and A. Sedrakian, Phys. Rev. Lett. **119**, 161104 (2017).
[20] A. Zacchi, M. Hanauske, and J. Schaffner-Bielich, Phys. Rev. D **93**, 065011 (2016).
[21] D. E. Alvarez-Castillo, D. B. Blaschke, A. G. Grunfeld, and V. P. Pagura, Phys. Rev. D **99**, 063010 (2019).
[22] J. J. Li, A. Sedrakian, and M. Alford, Phys. Rev. D **101**, 063022 (2020).
[23] Q.-w. Wang, C. Shi, Y. Yan, and H.-S. Zong, arXiv:1912.02312.
[24] K. B. Fadafan, J. C. Rojas, and N. Evans, Phys. Rev. D **101**, 126005 (2020).
[25] D. Blaschke, H. Grigorian, and G. Röpke, Particles **3**, 477 (2020).
[26] J.-E. Christian and J. Schaffner-Bielich, Astrophys. J. Lett. **894**, L8 (2020).
[27] E. Benitez, J. Weller, V. Guedes, C. Chirenti, and M. C. Miller, Phys. Rev. D **103**, 023007 (2021).
[28] A. Parisi, C. V. Flores, C. H. Lenzi, C.-S. Chen, and G. Lugones, J. Cosmol. Astropart. Phys. 06 (2021) 042.
[29] Z. Sharifi, M. Bigdeli, and D. Alvarez-Castillo, Phys. Rev. D **103**, 103011 (2021).
[30] T. Deloudis, P. Koliogiannis, and C. Moustakidis, EPJ Web Conf. **252**, 06001 (2021).
[31] J. J. Li, A. Sedrakian, and M. Alford, Phys. Rev. D **104**, L121302 (2021).
[32] J.-E. Christian and J. Schaffner-Bielich, arXiv:2109.04191.
[33] V. P. Goncalves, J. C. Jimenez, and L. Lazzari, Eur. Phys. J. C **82**, 110 (2022).
[34] P. Espino and V. Paschalidis, Phys. Rev. D **105**, 043014 (2022).
[35] M. Dutra, O. Lourenço, and D. P. Menezes, Phys. Rev. C **93**, 025806 (2016); **94**, 049901(E) (2016).
[36] L. McLerran and S. Reddy, Phys. Rev. Lett. **122**, 122701 (2019).
[37] C. Xia, Z. Zhu, X. Zhou, and A. Li, Chin. Phys. C **45**, 055104 (2021).

[38] T. Yazdizadeh and G. H. Bordbar, Iran. J. Sci. Technol. A **43**, 2691 (2019).
[39] M. Shahrbaf, D. Blaschke, A. G. Grunfeld, and H. R. Moshfegh, Phys. Rev. C **101**, 025807 (2020).
[40] A. Zacchi and J. Schaffner-Bielich, Phys. Rev. D **100**, 123024 (2019).
[41] T. Zhao and J. M. Lattimer, Phys. Rev. D **102**, 023021 (2020).
[42] L. L. Lopes and D. P. Menezes, Nucl. Phys. **A1009**, 122171 (2021).
[43] D. C. Duarte, S. Hernandez-Ortiz, and K. S. Jeong, Phys. Rev. C **102**, 025203 (2020).
[44] M. Rho, arXiv:2004.09082.
[45] M. Marczenko, Eur. Phys. J. Special Topics **229**, 3651 (2020).
[46] T. Minamikawa, T. Kojo, and M. Harada, Phys. Rev. C **103**, 045205 (2021).
[47] M. Hippert, E. S. Fraga, and J. Noronha, Phys. Rev. D **104**, 034011 (2021).
[48] R. D. Pisarski, Phys. Rev. D **103**, L071504 (2021).
[49] S. Sen and L. Sivertsen, Astrophys. J. **915**, 109 (2021).
[50] J. R. Stone, V. Dexheimer, P. A. M. Guichon, A. W. Thomas, and S. Typel, Mon. Not. R. Astron. Soc. **502**, 3476 (2021).
[51] M. Ferreira, R. C. Pereira, and C. Providência, Phys. Rev. D **102**, 083030 (2020).
[52] J. I. Kapusta and T. Welle, Phys. Rev. C **104**, L012801 (2021).
[53] R. Somasundaram and J. Margueron, arXiv:2104.13612.
[54] T. Kojo, AAPPS Bull. **31**, 11 (2021).
[55] A. Mukherjee, S. Schramm, J. Steinheimer, and V. Dexheimer, Astron. Astrophys. **608**, A110 (2017).
[56] V. Dexheimer, Pub. Astron. Soc. Aust. **34**, e066 (2017).
[57] A. Li, Z. Y. Zhu, E. P. Zhou, J. M. Dong, J. N. Hu, and C. J. Xia, J. High Energy Astrophys. **28**, 19 (2020).
[58] J. C. Jiménez and E. S. Fraga, Phys. Rev. D **104**, 014002 (2021).
[59] H.-M. Jin, C.-J. Xia, T.-T. Sun, and G.-X. Peng, arXiv: 2108.12736.
[60] H. K. Lee, Y.-L. Ma, W.-G. Paeng, and M. Rho, Mod. Phys. Lett. A **37**, 2230003 (2022).
[61] A. R. Raduta, F. Nacu, and M. Oertel, Eur. Phys. J. A **57**, 329 (2021).
[62] M. Dutra, O. Lourenco, J. S. Sa Martins, A. Delfino, J. R. Stone, and P. D. Stevenson, Phys. Rev. C **85**, 035201 (2012).
[63] V. A. Dexheimer and S. Schramm, Phys. Rev. C **81**, 045201 (2010).
[64] V. Dexheimer and S. Schramm, Astrophys. J. **683**, 943 (2008).
[65] P. A. M. Guichon, K. Saito, E. N. Rodionov, and A. W. Thomas, Nucl. Phys. **A601**, 349 (1996).
[66] G. Malfatti, M. G. Orsaria, I. F. Ranea-Sandoval, G. A. Contrera, and F. Weber, Phys. Rev. D **102**, 063008 (2020).
[67] P. Bedaque and A. W. Steiner, Phys. Rev. Lett. **114**, 031103 (2015).
[68] E. Annala, T. Gorda, A. Kurkela, J. Nättilä, and A. Vuorinen, Nat. Phys. **16**, 907 (2020).
[69] V. Dexheimer, R. O. Gomes, T. Klähn, S. Han, and M. Salinas, Phys. Rev. C **103**, 025808 (2021).
[70] J. R. Stone, V. Dexheimer, P. A. M. Guichon, A. W. Thomas, and S. Typel, Mon. Not. R. Astron. Soc. **502**, 3476 (2021).
[71] M. E. Gusakov, P. Haensel, and E. M. Kantor, Mon. Not. R. Astron. Soc. **439**, 318 (2014).
[72] M. G. de Paoli and D. P. Menezes, Adv. High Energy Phys. **2014**, 479401 (2014).
[73] D. Sen, Phys. Rev. C **103**, 045804 (2021).
[74] Z.-H. Tu and S.-G. Zhou, Astrophys. J. **925**, 16 (2022).
[75] D. Blaschke and D. Alvarez-Castillo, Eur. Phys. J. A **56**, 124 (2020).
[76] G. Montana, L. Tolos, M. Hanauske, and L. Rezzolla, Phys. Rev. D **99**, 103009 (2019).
[77] T. Kojo, AIP Conf. Proc. **2127**, 020023 (2019).
[78] G. Malfatti, M. G. Orsaria, G. A. Contrera, F. Weber, and I. F. Ranea-Sandoval, Phys. Rev. C **100**, 015803 (2019).
[79] N. Jokela, M. Järvinen, G. Nijs, and J. Remes, Phys. Rev. D **103**, 086004 (2021).
[80] K. S. Jeong, L. McLerran, and S. Sen, Phys. Rev. C **101**, 035201 (2020).
[81] S. Sen and N. C. Warrington, Nucl. Phys. **A1006**, 122059 (2021).
[82] A. Motornenko, J. Steinheimer, V. Vovchenko, S. Schramm, and H. Stoecker, Phys. Rev. C **101**, 034904 (2020).
[83] G. Baym, S. Furusawa, T. Hatsuda, T. Kojo, and H. Togashi, Astrophys. J. **885**, 42 (2019).
[84] C.-M. Li, J.-L. Zhang, Y. Yan, Y.-F. Huang, and H.-S. Zong, Phys. Rev. D **97**, 103013 (2018).
[85] D. Kumar, H. Mishra, and T. Malik, arXiv:2110.00324.
[86] M. Marczenko, K. Redlich, and C. Sasaki, Astrophys. J. Lett. **925**, L23 (2022).
[87] V. Dexheimer, G. Pagliara, L. Tolos, J. Schaffner-Bielich, and S. Schramm, Eur. Phys. J. A **38**, 105 (2008).
[88] K. Chatziioannou, C.-J. Haster, and A. Zimmerman, Phys. Rev. D **97**, 104036 (2018).
[89] B. P. Abbott *et al.* (LIGO Scientific, Virgo Collaborations), Phys. Rev. Lett. **121**, 161101 (2018).
[90] E. Chabanat, P. Bonche, P. Haensel, J. Meyer, and R. Schaeffer, Nucl. Phys. **A635**, 231 (1998); **A643**, 441 (1998).
[91] F. Douchin, P. Haensel, and J. Meyer, Nucl. Phys. **A665**, 419 (2000).
[92] F. Douchin and P. Haensel, Phys. Lett. B **485**, 107 (2000).
[93] H. Tan, J. Noronha-Hostler, and N. Yunes, Phys. Rev. Lett. **125**, 261104 (2020).
[94] V. Dexheimer, R. de Oliveira Gomes, S. Schramm, and H. Pais, J. Phys. G **46**, 034002 (2019).
[95] H. Pais and C. Providência, Phys. Rev. C **94**, 015808 (2016).
[96] E. Witten, Phys. Rev. D **30**, 272 (1984).
[97] P. Haensel, J. L. Zdunik, and R. Schaeffer, Astron. Astrophys. **160**, 121 (1986), https://inspirehep.net/literature/243725.

[98] T. E. Riley *et al.*, Astrophys. J. Lett. **887**, L21 (2019).
[99] M. C. Miller *et al.*, Astrophys. J. Lett. **887**, L24 (2019).
[100] T. E. Riley *et al.*, Astrophys. J. Lett. **918**, L27 (2021).
[101] M. C. Miller *et al.*, Astrophys. J. Lett. **918**, L28 (2021).
[102] See Supplemental Material at http://link.aps.org/supplemental/10.1103/PhysRevLett.128.161101 for some further explanation for the appearance of BLR curves.
[103] Z. Carson, K. Chatziioannou, C.-J. Haster, K. Yagi, and N. Yunes, Phys. Rev. D **99**, 083016 (2019).
[104] K. Yagi and N. Yunes, Classical Quantum Gravity **34**, 015006 (2017).